Peeling of thick adhesive interfaces: the role of dynamics and geometrical nonlinearity

Gregorio Mariggiò[a], José Reinoso[b], Marco Paggi[c], Mauro Corrado[a,*]

[a] *Department of Structural, Geotechnical and Building Engineering, Politecnico di Torino, Corso Duca degli Abruzzi 24, 10129 Torino, Italy*
[b] *School of Engineering, Universidad de Sevilla, Camino de los Descubrimientos s/n, 41092 Seville, Spain*
[c] *IMT School for Advanced Studies Lucca, Piazza San Francesco 19, 55100 Lucca, Italy*

Abstract

The present investigation addresses the simulation of layer debonding along thick interfaces in dynamic regime by means of the use of a cohesive interface model accounting for geometrical and material nonlinear effects. This novel approach is performed within the finite element framework. Numerical examples assess the influence of different interface parameters such as the adhesive thickness and the effect of the load line displacement velocity using a 90° peeling test. Current results pinpoint the relevance of the simultaneous consideration of both geometric and material nonlinear effects, which can notably alter the peak-force and the post-peak response evolution of the system in dynamic applications.

Keywords: Nonlinear fracture mechanics, Dynamics, Finite thickness interfaces, Cohesive zone model, Large displacements

1. Introduction

The problem of dynamic fracture along interfaces is particularly relevant in applications involving thin structural elements subjected to large displacements, such as biological membranes, thin-films and coatings, paper sheets, elastomers, and viscoelastic materials, among many other systems. In these cases, the modelling complexity relies on the fact that, during the simulation, the deformed configuration cannot be approximated by the undeformed one any longer due to the development of geometric nonlinear effects (which may concomitantly occur with material nonlinearities). Hence, the relative rotations between the two flanks of the interface and the simultaneous deformation of the two bodies separated by the interface should be tracked throughout the simulations process. Moreover, in many practical situations, the thickness of the interface is often not negligible in comparison to that corresponding to the bonded layers. In spite of these considerations, interfaces can be modelled with zero-thickness interface elements having a cohesive response, although generalized to take into account the interface finite-thickness properties. In statics, for instance, an equivalence between the finite-thickness interface with damage mechanics and a zero-thickness interface whose mechanical response is ruled by a novel type of cohesive zone model (CZM) was thoroughly investigated in [1, 2]. In dynamics, the mass effect of thick interfaces on the dynamic characteristics of laminated composites was investigated in [3]. The possibility to design metamaterials with unusual filtering characteristics was suggested in [4], with the use of truss-like micro-structured interfaces. Recently, the effect of the interface mass on nonlinear fracture of laminates in a dynamic regime was studied in [5].

With regard to the problem of the combined effect of material and geometrical nonlinearities, a number of alternative formulations for 2D and 3D interface elements in large displacements has been proposed following different approaches (see updated Lagrangian formulation developed in [6, 7, 8], the beam-like conception in [9, 10], and the co-rotational model in [11], to quote a few of them).

In the present study, the consistent interface finite element (FE) formulation for material and geometrical nonlinearities proposed by Reinoso and Paggi [12] is extended for the simulation of layer debonding along thick interfaces in dynamic regime. In Section 2.1, the formulation of an interface element for finite thickness structural interfaces undergoing large displacements is outlined. The constitutive relationships for the intrinsic CZM approach are introduced in Section 2.2, whilst the numerical approach is applied in Section 3 to the 90° peeling test. Conclusions are drawn in Section 4.

2. Interface model and FE formulation

2.1. Equations of motion and finite element approximation

Let us to consider two deformable bodies with volumes $V_{1,2}$ and external boundaries $\partial V_{1,2}$, connected by a cohesive interface S. The dynamic FE formulation accounting for combined cohesive and dynamic effects can be expressed through the advocation of the Principle of Virtual

---

*Corresponding author
Email address: mauro.corrado@polito.it (Mauro Corrado)

Work (PVW):

$$\delta\Pi(\mathbf{u}, \boldsymbol{\eta}) = \int_{V_{1,2}} (\nabla\boldsymbol{\eta})^{\mathrm{T}} \boldsymbol{\sigma} \, dV - \int_{V_{1,2}} \boldsymbol{\eta}^{\mathrm{T}} \rho_v \ddot{\mathbf{u}} \, dV -$$
$$\int_{\partial V_{1,2}} \boldsymbol{\eta}^{\mathrm{T}} \mathbf{f} \, dS - \int_S \delta\mathbf{g}_{\mathrm{loc}}^{\mathrm{T}} \mathbf{T} \, dS - \int_S \boldsymbol{\eta}^{\mathrm{T}} \rho t \ddot{\mathbf{u}} \, dS = 0 \quad (1)$$

where $\left\{ \boldsymbol{\eta} \in [H^1(\mathcal{B}_0)] : \boldsymbol{\eta} = \mathbf{0} \text{ on } \partial V_{1,2}, u \right\}$ is the compatible virtual displacement field, with $\partial V_{1,2}, u$ the portion of the boundary with prescribed displacements. Moreover in Eq.(1), the first term is the internal virtual work of deformation of the adjoint bulk bodies, the second term indicates the work done by dynamic forces (ρ_v is the mass density of the bodies and $\ddot{\mathbf{u}}$ are the accelerations), the third term is the virtual work of the tractions $\mathbf{f}$ acting on the boundaries of the bodies $\partial V_{1,2}$, the fourth term represents the contribution of the interface cohesive tractions $\mathbf{T} = (\tau, \sigma)^{\mathrm{T}}$, acting on S, in which the gap vector $\mathbf{g}_{\mathrm{loc}} = (g_{\mathrm{t}}, g_{\mathrm{n}})^{\mathrm{T}}$, computed in a local frame defined by the tangential and the normal directions referred to the updated mid-line of the interface element represents the relative sliding and opening displacements between the two flanks of the interface. The last term in Eq.(1) is the finite thickness contribution to the work by dynamic forces (ρ and t identify the density mass and the thickness of the cohesive interface, respectively). The virtual variation of the contribution of the interface cohesive tractions to the PVW reads:

$$\delta\Pi_{\mathrm{intf}}(\mathbf{g}_{\mathrm{loc}}, \boldsymbol{\eta}) = \boldsymbol{\eta}^{\mathrm{T}} \int_S \left(\frac{\partial\mathbf{g}_{\mathrm{loc}}}{\partial\boldsymbol{\eta}} \right)^{\mathrm{T}} \mathbf{T}(\mathbf{g}_{\mathrm{loc}}) \, dS \quad (2)$$

The gap vector in the global Cartesian frame, $\mathbf{g}$, can be obtained by multiplying a suitable operator $\mathbf{L}$, that provides the difference between the displacements of the upper and the lower bodies at the interface, with the vector of the nodal displacements $\mathbf{d}$ associated with the underlying spatial discretization using FEM:

$$\mathbf{g} \cong \mathbf{g}^{\mathrm{e}} = \mathbf{N}\mathbf{L}\mathbf{d} \quad (3)$$

where $\mathbf{N}$ is the operator that collects the shape functions. Advocating a standard isoparametric approach, the partial derivative in Eq. (2) is approximated by:

$$\frac{\partial\mathbf{g}_{\mathrm{loc}}}{\partial\boldsymbol{\eta}} \cong \frac{\partial\mathbf{g}_{\mathrm{loc}}^{\mathrm{e}}}{\partial\mathbf{d}} = \mathbf{R}(\mathbf{d})\mathbf{N}\mathbf{L} + \frac{\partial\mathbf{R}(\mathbf{d})}{\partial\mathbf{d}}\mathbf{N}\mathbf{L}\mathbf{d} \quad (4)$$

where the operator $\mathbf{R}(\mathbf{d})$, which is function of the displacement field $\mathbf{d}$ in the large displacement setting, is the rotation operator which pre-multiplies the gap vector in the global frame and yields the gap vector in local frame, $\mathbf{g}_{\mathrm{loc}}$. The expression of $\mathbf{R}(\mathbf{d})$ for a 4-node interface element is detailed in [12] along with the expressions for $\mathbf{L}$ and $\mathbf{N}$.

Introducing the operator $\mathbf{B} = \mathbf{N}\mathbf{L}$, Eq. (4) becomes:

$$\frac{\partial\mathbf{g}_{\mathrm{loc}}^{\mathrm{e}}}{\partial\mathbf{d}} = \mathbf{R}\mathbf{B} + \frac{\partial\mathbf{R}}{\partial\mathbf{d}}\mathbf{B}\mathbf{d} \quad (5)$$

Equation (2) can be rewritten by introducing the discretization of the interface as:

$$\delta\Pi_{\mathrm{intf}}^{e} = \delta\mathbf{d}^{\mathrm{T}} \int_S \left(\mathbf{R}\mathbf{B} + \frac{\partial\mathbf{R}}{\partial\mathbf{d}}\mathbf{B}\mathbf{d} \right)^{\mathrm{T}} \mathbf{T} \, dS \quad (6)$$

The solution of the variational equation $\delta\Pi_{\mathrm{intf}}^{e} = \delta\mathbf{d}^{\mathrm{T}} \mathbf{f}_{\mathrm{intf}}^{e,k} = 0 \, \forall \, \delta\mathbf{d}$ results in the equations set $\mathbf{f}_{\mathrm{intf}}^{e,k} = \mathbf{0}$, where $\mathbf{f}_{\mathrm{intf}}^{e,k}$ is a non linear function of the unknown $\mathbf{d}$ and it assumes the role of the residual vector in the Newton-Raphson iterative scheme:

$$\mathbf{f}_{\mathrm{intf}}^{e,k} = \int_S \left(\mathbf{R}\mathbf{B} + \frac{\partial\mathbf{R}}{\partial\mathbf{d}}\mathbf{B}\mathbf{d} \right)^{\mathrm{T}} \mathbf{T} \, dS \quad (7)$$

which leads to the following equations set for the computation of the correction $\Delta\mathbf{d}$ at each iteration k:

$$\mathbf{K}^{e,k}\Delta\mathbf{d} = -\mathbf{f}_{\mathrm{intf}}^{e,k} \quad (8)$$

Omitting the superscript k in order to alleviate the notation, the element stiffness matrix $\mathbf{K}^{\mathrm{e}}$ is given by the linearization of the residual. This operator, $\mathbf{K}^{\mathrm{e}}$, is evaluated by using the displacement field solution at the iteration k:

$$\mathbf{K}^e = \int_S 2\mathbf{B}^{\mathrm{T}} \frac{\partial\mathbf{R}^{\mathrm{T}}}{\partial\mathbf{d}} \mathbf{T}$$
$$+ \left(\mathbf{B}^{\mathrm{T}}\mathbf{R}^{\mathrm{T}} + \mathbf{d}^{\mathrm{T}}\mathbf{B}^{\mathrm{T}}\frac{\partial\mathbf{R}^{\mathrm{T}}}{\partial\mathbf{d}} \right) \frac{\partial\mathbf{T}}{\partial\mathbf{d}} \, dS \quad (9)$$

The derivative of the cohesive traction vector $\mathbf{T}$ with respect to the displacement vector $\mathbf{d}$ reads:

$$\frac{\partial\mathbf{T}}{\partial\mathbf{d}} = \frac{\partial\mathbf{T}}{\partial\mathbf{g}_{\mathrm{loc}}} \frac{\partial\mathbf{g}_{\mathrm{loc}}}{\partial\mathbf{d}} = \mathbf{C} \left(\mathbf{R}\mathbf{B} + \frac{\partial\mathbf{R}}{\partial\mathbf{d}}\mathbf{B}\mathbf{d} \right) \quad (10)$$

After some manipulations, the stiffness matrix contributions related to material and geometric nonlinearities render

$$\mathbf{K}^e = \mathbf{K}_{\mathrm{mat}}^e + \mathbf{K}_{\mathrm{geom}}^e \quad (11\mathrm{a})$$

with

$$\mathbf{K}_{\mathrm{mat}}^e = \int_S \mathbf{B}^{\mathrm{T}}\mathbf{R}^{\mathrm{T}}\mathbf{C}\mathbf{R}\mathbf{B} \, dS \quad (11\mathrm{b})$$

$$\mathbf{K}_{\mathrm{geo}}^e = \int_S 2\mathbf{B}^{\mathrm{T}}\frac{\partial\mathbf{R}^{\mathrm{T}}}{\partial\mathbf{d}}\mathbf{T} + \mathbf{d}^{\mathrm{T}}\mathbf{B}^{\mathrm{T}}\frac{\partial\mathbf{R}^{\mathrm{T}}}{\partial\mathbf{d}}\mathbf{C}\frac{\partial\mathbf{R}}{\partial\mathbf{d}}\mathbf{B}\mathbf{d}$$
$$+ \left(\mathbf{B}^{\mathrm{T}}\mathbf{R}^{\mathrm{T}}\mathbf{C}\frac{\partial\mathbf{R}}{\partial\mathbf{d}}\mathbf{B}\mathbf{d} + \mathbf{d}^{\mathrm{T}}\mathbf{B}^{\mathrm{T}}\frac{\partial\mathbf{R}^{\mathrm{T}}}{\partial\mathbf{d}}\mathbf{C}\mathbf{R}\mathbf{B} \right) dS \quad (11\mathrm{c})$$

Within the FE discretization, the governing equation (Eq. (1)) in matrix form becomes:

$$\mathbf{M}\ddot{\mathbf{d}} + \mathbf{f}_{\mathrm{int}} = \mathbf{f}_{\mathrm{ext}} \quad (12)$$

where $\mathbf{M}$ is a lumped mass matrix, $\mathbf{f}_{\text{int}}$ is the internal force vector obtained from the multiplication between the tangent stiffness matrix, provided by Eq. (11a), and the vector of nodal displacements $\mathbf{d}$. The external force vector $\mathbf{f}_{\text{ext}}$ is related to the surface tractions acting on the boundaries $\partial V_{1,2}$.

Regarding the mass matrix of the interface element, $\mathbf{M}_{\text{intf}}$, here it is taken into account via a lumped approximation. The mass of the interfaces is then assembled into the global mass matrix of the system $\mathbf{M}$.

2.2. Cohesive fracture law

In this investigation, we particularized the interface behavior using a cohesive zone model (CZM) that is characterized by a linear ascending branch followed by an exponential softening in order to simulate the phenomenon of layer debonding. Note that following the previous formulation, the current interface accounts for finite thickness properties of the adhesive and the geometrical second order effects. In this concern, the initial slope of the linear branch prior softening, K, can be estimated as the ratio between the Young's modulus (E_{adh}) and the thickness of the adhesive, i.e. $K = E_{\text{adh}}/t$. A formulation for mixed mode crack propagation, i.e. with coupling between normal and tangential cohesive tractions, is used:

$$
\sigma = \begin{cases} \sigma_{\max} e^{\left(\dfrac{-l_0 - |g_t|}{r}\right)} \dfrac{g_n}{l_0}, & \text{if } 0 \leq \dfrac{g_n}{r} < \dfrac{l_0}{r} \\[2ex] \sigma_{\max} e^{\left(\dfrac{-g_n - |g_t|}{r}\right)}, & \text{if } \dfrac{l_0}{r} \leq \dfrac{g_n}{r} < \dfrac{g_{nc}}{r} \\[2ex] 0, & \text{if } \dfrac{g_n}{r} \geq \dfrac{g_{nc}}{r} \end{cases} \tag{13}
$$

$$
\tau = \begin{cases} \tau_{\max} e^{\left(\dfrac{-l_0 - g_n}{r}\right)} \dfrac{g_t}{l_0}, & \text{if } 0 \leq \dfrac{|g_t|}{r} < \dfrac{l_0}{r} \\[2ex] \tau_{\max} e^{\left(\dfrac{-g_n - |g_t|}{r}\right)} \text{sgn}(g_t), & \text{if } \dfrac{l_0}{r} \leq \dfrac{|g_t|}{r} < \dfrac{g_{tc}}{r} \\[2ex] 0, & \text{if } \dfrac{|g_t|}{r} \geq \dfrac{g_{tc}}{r} \end{cases} \tag{14}
$$

where g_n and g_t are the relative opening and sliding displacements of the crack. In the present model, the selection of the initial stiffness is made by varying the internal parameter l_0, which defines the opening and sliding displacements corresponding to the peak CZM tractions before the onset of the exponential softening. The parameter $\sigma_{\max}$ in Eq. 13 is the maximum tensile cohesive traction, achievable in the limit case of $l_0 = 0$. On the other hand, the real peak value of the CZM law is $\sigma_p = \sigma_{\max} \exp(-l_0/R)$. The same holds for the tangential component. The other parameters entering the formulation in Eq. 13 and 14 are the critical opening and sliding displacement, g_{nc} and g_{tc}, corresponding to complete

cracking in pure Mode I and Mode II loading, and an internal characteristic length scale related to the roughness of the fractured interface, r. In the present formulation, the ascending branch is treated separately from the softening one, thus allowing to change the initial stiffness, the cohesive fracture energy and the peak stress independently from each other. In compression, a penalty formulation is used, with a penalty parameter p_n equal to the stiffness K in tension.

3. Applications: numerical investigation

In order to illustrate the performance of the proposed model, a 90° peeling test is analyzed as a case study, whereby a thin layer is pulled from a rigid substrate by the action of a vertical displacement imposed to one of its ends. The horizontal and vertical displacements are restrained along the lower and the left edges of the substrate. The sketch of the current system and its dimensions are shown in Fig. 1. From the top side to the bottom, the stack of layers consists of a 0.3 mm thick polymeric lamina, an adhesive of thickness t and mass density ρ, and a 4 mm thick glass substrate. The polymeric material, obeying a Neo-Hookean hyperelastic material law, is characterized by: Young's modulus $E_{\text{poly}} = 2.8$ GPa, Poisson's ratio $\nu = 0.2$, and mass density $\rho_{\text{poly}} = 2000$ kg/m^3. The glass has a Young's modulus $E_{\text{glass}} = 73$ GPa, Poisson's ratio $\nu_{\text{glass}} = 0.22$, and a mass density $\rho_{\text{glass}} = 2500$ kg/m^3. It has a linear elastic constitutive behaviour. The adhesive layer is modelled as a finite thickness interface, with the aforementioned CZM formulation to account for its finite thickness. Its mechanical properties are: Young's modulus $E_{\text{adh}} = 6.6$ MPa, tensile strength $\sigma_{\text{peak}} = 5.80$ MPa, critical opening displacement in Mode I $g_{\text{nc}} = 2.5$ mm, fracture energy $G_{\text{F}} = 4850$ N/m. The same properties are used for Mode II.

A plane strain FE model is considered with 4-node isoparametric quadrangular finite elements with linear shape functions for the discretization of the continuum. The same interpolation order is used for the interface finite elements. The glass substrate has a length of 50 mm, and it is discretized with 200x18 elements (element size 250x220 μm), whereas the lamina is discretized with 200x4 elements (element size 250x75 μm). The cohesive zone length, function of the material properties according to the relationship provided in [13], is about 1 mm. Therefore, at least four interface elements are used within the cohesive zone in order to properly describe stress transfer within the process zone size. The numerical simulations are performed under the assumption of both small and large displacements for the adhesive layer, by imposing a load-line displacement at the top right corner of the peeled layer with a prescribed velocity v. However, instead of imposing the prescribed constant velocity from the very beginning of the simulation, a ramp function is considered to provide a smooth transition from the initial configuration to the steady-state velocity, see Fig. 2. The velocity
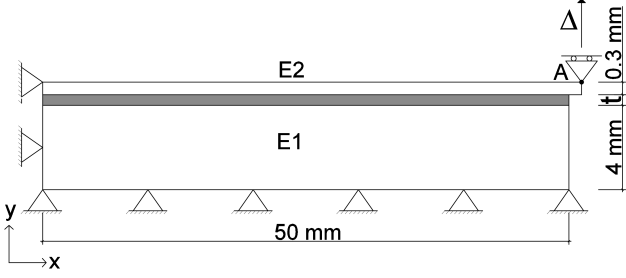
Figure 1: Sketch of the peeling test.

ramp extends over 30 μs and is defined in order to have a vanishing acceleration at starting time and at 30 μs. The steady-state velocity is reached at 30 μs. The introduction of this ramp function was found to be essential to avoid spurious vibrations without introducing viscous damping in the system. At each time step, the solution of the equilibrium equations is achieved by the Newton–Raphson method. Integration in time is performed by the Newmark constant-average-acceleration scheme ($\beta = 0.5$, $\gamma = 0.25$) with a time step $\Delta t = 2\ \mu$s.

(a)
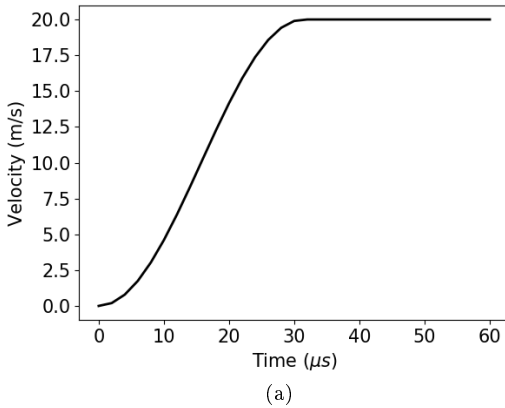
Figure 2: Ramp function for the imposed load-line velocity.

3.1. Small vs. large displacement formulation

The first set of simulations concerns the comparison between the small and large displacement formulations for the interface elements, in both quasi-static and dynamic loading conditions. To this purpose, the adhesive thickness and mass density are set equal to 0.4 mm and 2000 kg/m^3, respectively, and a steady-state velocity of 20 m/s is used for the dynamic simulations. The numerical predictions relating the peeling force, i.e. the vertical reaction in the point A (Fig. 1), to the load-line displacement are shown in Fig. 3. As a general trend, the large displacement formulation for the interface elements leads to peak loads higher than those obtained with the small displacement formulation. Such results are in line with those recently obtained in statics by Reinoso and Paggi [12], and now

are extended to the dynamic regime. Furthermore, the dynamic effect on the peak load observed by Corrado and Paggi [5] in layer debonding in laminates with small displacement formulation is herein confirmed in the presence of geometrical nonlinearities. For the present case-study, the combined effect of geometrical nonlinearity and dynamics leads to an increase of the peak load of about 25% as compared to the quasi-static simulation in the hypothesis of small displacements.
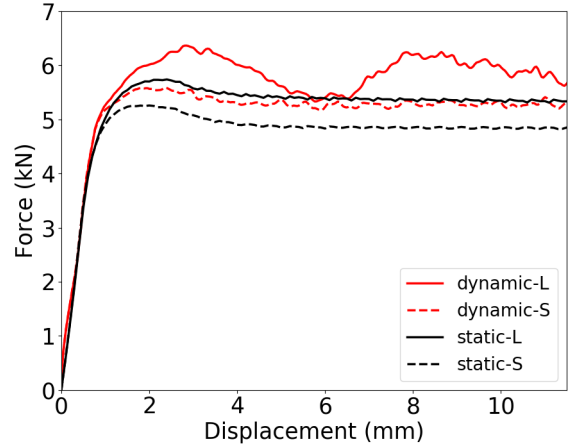

Figure 3: Peeling force vs. load-line displacement curves for quasi-static and dynamic loading conditions, and different kinematic formulations for the interface elements (S stands for small displacements; L stands for large displacements).

Besides the peak load, which has the maximum amplification among all the cases shown in Fig. 3, the load-displacement curve for the "dynamic-L" case differs from the rest in the shape of the post-peak branch, characterized by a broad oscillation having a period of about 300 μs (see Fig. 4, where the peeling force is plotted as a function of time). This oscillation of the external reaction is a direct consequence of the fact that, in the large displacement formulation, the evolution of the interface deformation is triggered throughout the simulation and therefore the interface geometry is updated. Thus, due to the progress of the debonding process, the middle line of the interface element rotates from the original horizontal direction toward the vertical one. Consequently, the vertical peeling force gives two traction contributions to the cohesive elements: a normal traction that promotes layer debonding, and a tangential traction (see Fig. 5 for its graphical visualization). In a dynamic regime, the latter component activates an axial vibration in the peeled layer, thus producing the global oscillation in the peeling force evidenced in Figs. 3 and 4. To confirm this hypothesis, the frequency of the first axial vibration mode of the lamina has been computed. Its value is equal to 270 μs , very close to the period of the obtained oscillation (see Fig. 4). Conversely, this oscillation was not captured in the case of small displacements formulation [5] because the equilibrium is imposed onto the undeformed state, where the middle line of the cohesive

4

elements keeps unmodified during the simulation. Therefore, the vertical peeling force does not produce traction components tangent to the interface elements.
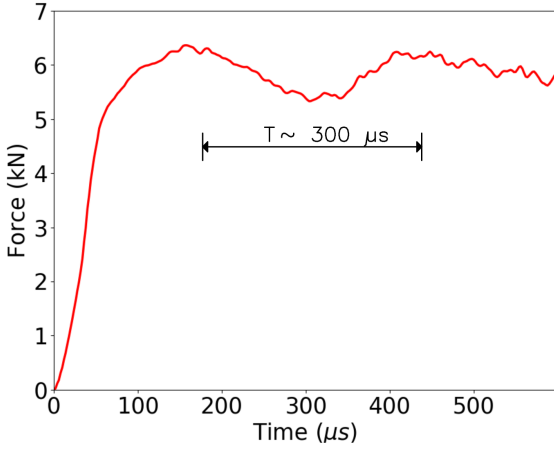

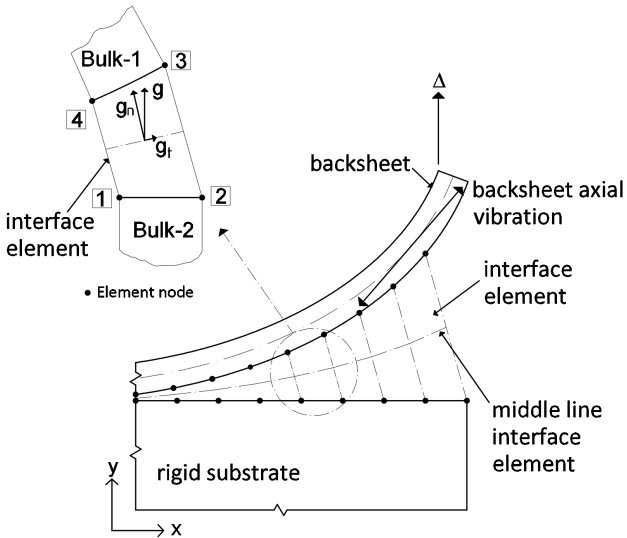Figure 4: Force vs. time curve.

Figure 5: Kinematics of interface elements under large displacements.

3.2. Effect of the load-line displacement velocity

A second set of numerical simulations are carried out in oder to analyze the effect of the load-line displacement velocity, v, on the debonding process with and without geometrical nonlinearity. In this case, the thickness and the mass density of the adhesive layer are set equal to 0.4 mm and 1200 kg/m^3, respectively, whereas three different load-line displacement velocities are examined: 10, 20 and 30 m/s. The load-displacement curves are shown in Fig. 6(a) for small displacements and in Fig. 6(b) for large displacements.

By increasing the velocity v, an increase in the peak load is observed. This is the result of the interplay between

the CZM properties and the inertia forces and it is not related to rate-dependent parameters. The dynamic increase factor, DIF, computed as the ratio between the peak load in dynamic regime and the peak load from the quasi-static simulation, is computed and depicted in Fig. 6(c), for both small and large displacements formulations. Such a ratio is an increasing function of the imposed velocity and it ranges from 1.0 to 1.21 in the explored velocity range. Hence, the effect of the kinematic formulation on the DIF is not negligible, since the geometrical nonlinearity leads to higher values of DIF for the same velocity, as compared to the small displacement formulation.

3.3. Effect of the adhesive thickness

The effect of the adhesive thickness is illustrated in Fig. 7 for an adhesive with $\rho = 1200$ kg/m^3. A change of adhesive thickness results into a modification of the interface element stiffness K. In particular, since $K = E_{adh}/t$, thicker adhesives are more compliant than thinner ones. Three thicknesses, equal to 0.4 mm, 0.8 mm and 1.2 mm, are considered. The change in the initial stiffness of the cohesive law does not affect the peak cohesive traction and the fracture energy, which are kept constant in all the simulations.

According to the obtained results, in both quasi-static and dynamic analyses the peak load is an increasing function of t (see Fig. 7(a) for small displacements and Fig. 7(b) for large displacements). The DIF increases by increasing the layer thickness for $v = 20$ m/s with both small and large displacements formulations, as shown in Fig. 7(c). However, the dynamic effect on the peak load is amplified by the consideration of geometrical nonlinearities. While the combined effect of the layer thickness on the stiffness and the mass of the whole system is examined in Fig. 7, the pure effect of the mass of the adhesive interface is shown in Fig. 8, where the peeling forces, plotted as a function of the load-line displacements, are computed for $v = 20$ m/s, $t = 0.4$ mm, and different values of adhesive mass density ρ. The peak load and the post-peak response are only slightly influenced by ρ in the small displacements formulation (Fig. 8(a)), whereas its effect is amplified by the presence of the geometrical nonlinearity (Fig. 8(b)). Finally, Fig. 8(c) shows that the DIF increases almost linearly by varying the mass density from 0 kg/m^3 to 3600 kg/m^3, with a slope slightly higher in the case of large displacements formulation.

4. Conclusions

In the present paper, the nonlinear cohesive interface model proposed in [12] has been extended for the simulation of dynamic fracture along thick interfaces within the framework of FEM. The main novelty of the proposed interface model consists in accounting for the combination of material nonlinearity, geometric nonlinearity and interface inertia, which are included in a compact formulation
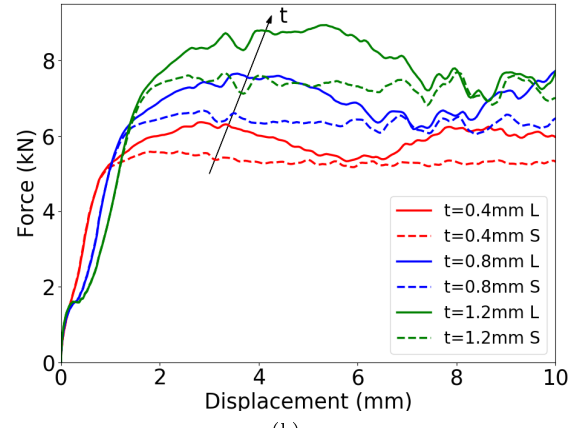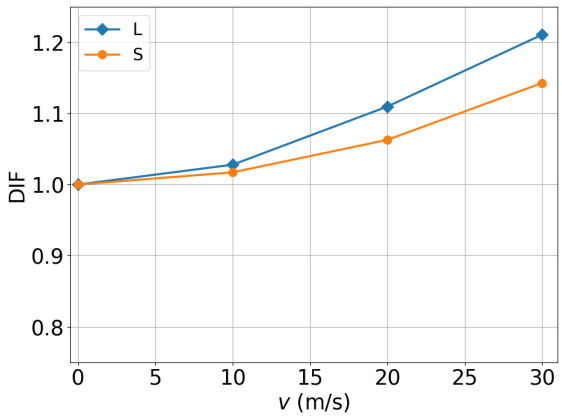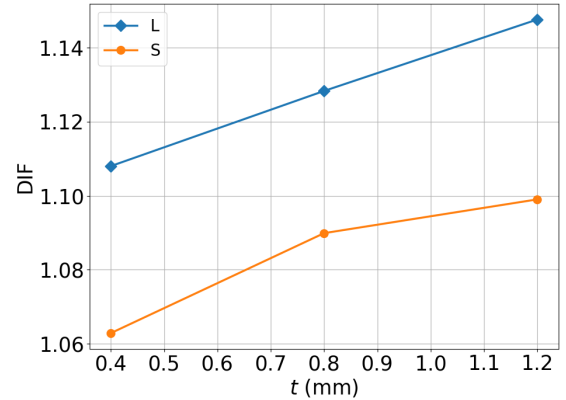
(a)

(b)
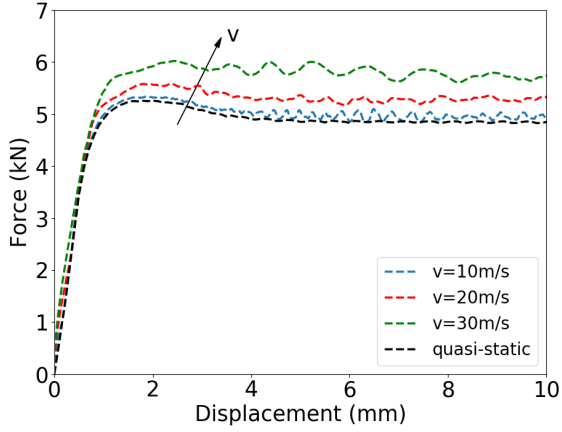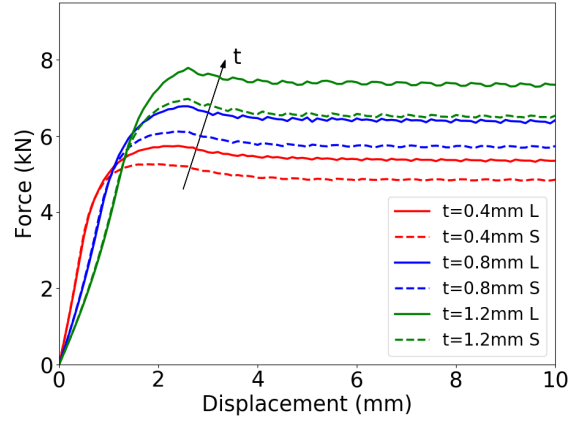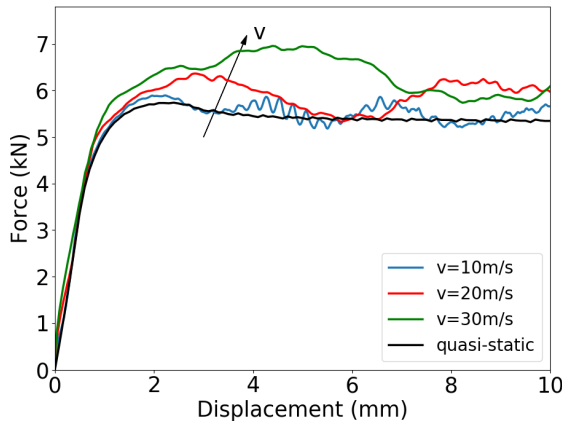
(c)

Figure 6: Effect of the load-line displacement velocity v on the peeling test for $t = 0.4$ mm and $\rho = 1200$ kg/m^3: (a) force vs. displacement curves for small displacement formulation for the interface elements; (b) force vs. displacement curves for large displacement formulation for the interface elements; (c) DIF vs. load-line velocity (S and L stand for small and large displacements, respectively).

(a)

(b)

(c)

Figure 7: Effect of the adhesive thickness t on the peeling test in small and large displacement formulations (S and L stand for small and large displacements, respectively): (a) statics; (b) dynamics ($v = 20$ m/s); (c) DIF vs. adhesive thickness.

that can be implemented in general purpose FE codes in a straightforward manner. Compared to the model proposed in [5], which applies to the dynamic debonding in the framework of small displacements, the current approach has an improved capability to predict the dynamic debonding in laminated composites made of soft hyperelastic layers and thick adhesive interfaces.
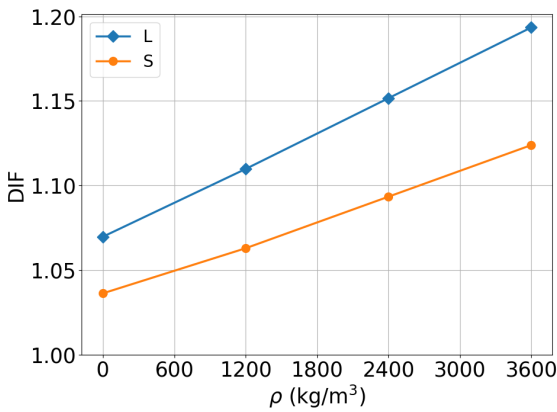
The performance of the proposed formulation has been assessed by examining the role of different parameters in a 90° peeling test in dynamic regime. First, the evaluation of the role of geometric nonlinearities evidenced that both the peak-force and the post-peak evolution of the

6
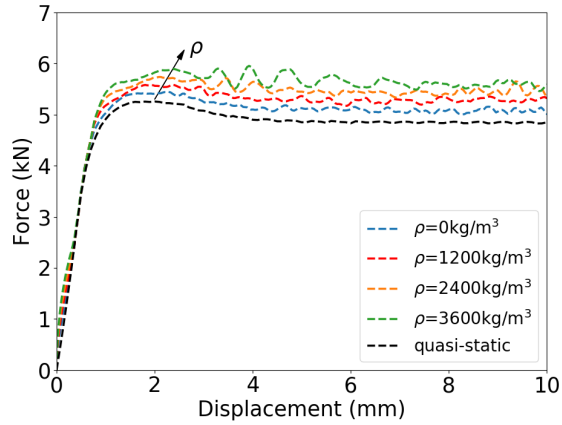
(a)
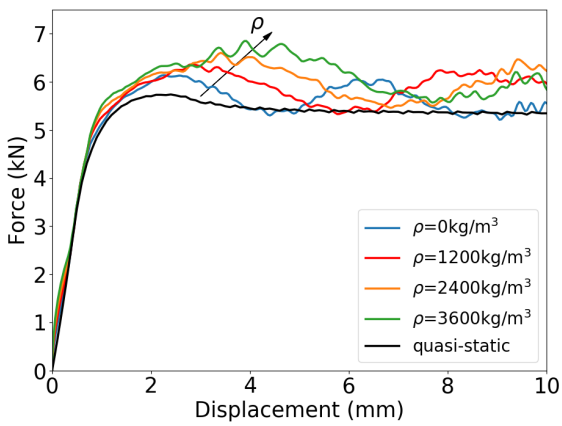
(b)

(c)

Figure 8: Effect of the adhesive mass density for $t = 0.4$ mm and $v = 20$ m/s: (a) small displacement formulation; (b) large displacement formulation; (c) DIF vs. adhesive mass density (S and L stand for small and large displacements, respectively).

system are affected by geometric effects. In particular, the predicted peak-force of the system for the geometrically nonlinear formulation is around 25% higher than that corresponding to the small displacements formulation. Moreover, the post-peak response corresponding to the former case showed an oscillatory pattern that is ascribed to the

activation of local mixed-mode fracture conditions at the adhesive.

In line with these results, the role of load-line displacement velocity of the system and the adhesive thickness was also examined. Both sets of simulations pinpoint a significant role of the consideration of the geometrical nonlinear effects leading to higher dynamic increase factors, which is a result of notable importance in many practical applications.

5. Acknowledgements

References

[1] M. Paggi, P. Wriggers, A nonlocal cohesive zone model for finite thickness interfaces. Part I: Mathematical formulation and validation with molecular dynamics, Comp. Mater. Sci. 50 (2011) 1625–1633.

[2] M. Paggi, P. Wriggers, A nonlocal cohesive zone model for finite thickness interfaces. Part II: FE implementation and application to polycrystalline materials, Comp. Mater. Sci. 50 (2011) 1634–1643.

[3] D. Bigoni, A. Movchan, Statics and dynamics of structural interfaces in elasticity, Int. J. Solids Struct. 39 (2002) 4843–4865.

[4] M. Brun, S. Guenneau, A. Movchan, D. Bigoni, Dynamics of structural interfaces: filtering and focussing effects for elastic waves, J. Mech. Phys. Solids 58 (2010) 1212–1224.

[5] M. Corrado, M. Paggi, Nonlinear fracture dynamics of laminates with finite thickness adhesives, Mech. Mater. 80 (2015) 183–192.

[6] M. Ortiz, A. Pandolfi, Finite deformation irreversible cohesive elements for three-dimensional crack-propagation analysis, Int. J. Numer. Meth. Eng. 44 (1999) 1267–1282.

[7] S. Roychowdhury, Y. Arun Roy, Ductile tearing in thin aluminium panels: experiments and analyses using large-displacement 3-d surface cohesive elements, Eng. Fract. Mech. 69 (2002) 983–1002.

[8] R. Fleischhauer, R. Behnke, M. Kaliske, A thermomechanical interface element formulation for finite deformations, Comput. Mech. 52 (2013) 1039–1058.

[9] M. van den Bosch, P. Schreurs, M. Geers, A cohesive zone model with a large displacement formulation accounting for interfacial fibrilation, Eur. J. Mech. A-Solid 26 (2007) 1–19.

[10] M. van den Bosch, P. Schreurs, M. Geers, On the development of a 3d cohesive zone element in the presence of large deformations, Comput. Mech. 42 (2008) 171–180.

[11] Y. Qiu, M. Crisfield, G. Alfano, An interface element formulation for the simulation of delamination with buckling, Eng. Fract. Mech. 68 (2001) 1755–1776.

[12] J. Reinoso, M. Paggi, A consistent interface element formulation for geometrical and material nonlinearities, Comput. Mech. 54 (2014) 1569–1581.

[13] J. Rice, The mechanics of earthquake rupture, in: A. Dziewonski, E. Boschi (Eds.), Physics of the Earth's interior - Proceedings International School of Physics 'Enrico Fermi', Course 78, Italian Physical Society and North-Holland Publ. Co., 1980, pp. 555–649.